

Experimental observation of plasma paramagnetism in a tokamak

D. J. Holly, S. C. Prager, M. W. Phillips, and J. C. Sprott

Department of Physics, University of Wisconsin, Madison, Wisconsin 53706
(Received 10 September 1979; accepted 12 November 1979)

The increase in the toroidal magnetic field of a tokamak due to plasma presence is measured experimentally and compared with predictions of an equilibrium code.

It is well known that tokamaks are diamagnetic at high β and paramagnetic at low β ; i.e., at low β the diamagnetic current ($\sim \nabla P \times \mathbf{B}/|B|^2$) is negligible, current flows parallel to the magnetic field ($\mathbf{j} \times \mathbf{B} = 0$) and the poloidal component of the parallel current causes the toroidal magnetic field to increase from its vacuum value. This feature of the equilibrium has not been reported experimentally. It is to be distinguished from the type of paramagnetism that arises in some systems when the plasma-induced current ($\nabla P \times \mathbf{B}/|B|^2$) is in such a direction as to increase the field. Numerical calculation¹ indicates that the boundary between paramagnetism and diamagnetism in a tokamak is roughly $\beta_p \approx 1$, where $\beta_p \equiv 8\pi \langle \langle P \rangle_v - p_0 \rangle / \langle B_p^2 \rangle_s$, p_0 is the pressure at the plasma edge, B_p is the poloidal magnetic field, and $\langle \rangle_v$ and $\langle \rangle_s$ represent averages over the plasma volume and surface, respectively.

Here, we report observations of the paramagnetic effect in the Tokapole II device,² a tokamak with a four-null poloidal divertor (Fig. 1). The plasma and field shaping is accomplished by four internal rings which create an octupole vacuum field. The temperature is sufficiently low ($T_e \sim 100$ eV, $n \sim 10^{13}$ cm⁻³, $I_p \sim 40$ kA, and $B_T \sim 3.5$ kG for this experiment) so that a magnetic probe may be inserted into the plasma without serious effect. The measured experimental ΔB_T is shown in Fig. 2. The poloidal current density on the midplane may be inferred from the data [$j_p \sim (1/R)(\partial B_T R)/\partial R$].

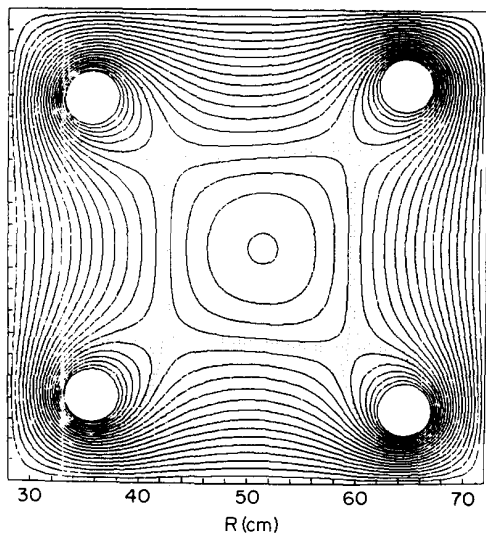


FIG. 1. Numerical poloidal flux plot of Tokapole II.

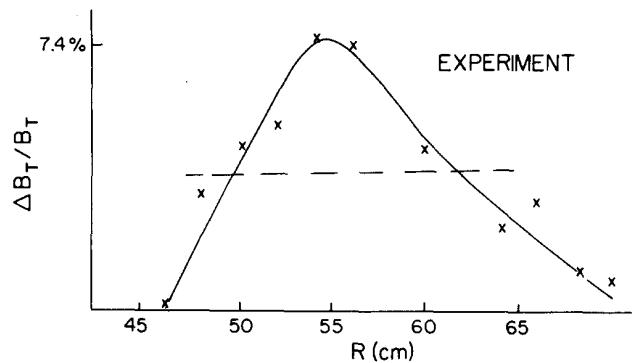


FIG. 2. Experimental measurement of $\Delta B_T/B_T$ vs distance from main axis. Measurement from the dashed baseline eliminates the contribution from the poloidal current in the scrape-off region.

Results are compared with an equilibrium code which solves the Grad-Shafranov equation

$$\Delta^* \psi = \partial^2 \psi / \partial r^2 - (1/r) \partial \psi / \partial r + \partial^2 \psi / \partial z^2 = -\mu_0 r^2 p'(\psi) - FF'(\psi)$$

for tokapole geometry. Since $\beta_p \approx 0.2$ in the experi-

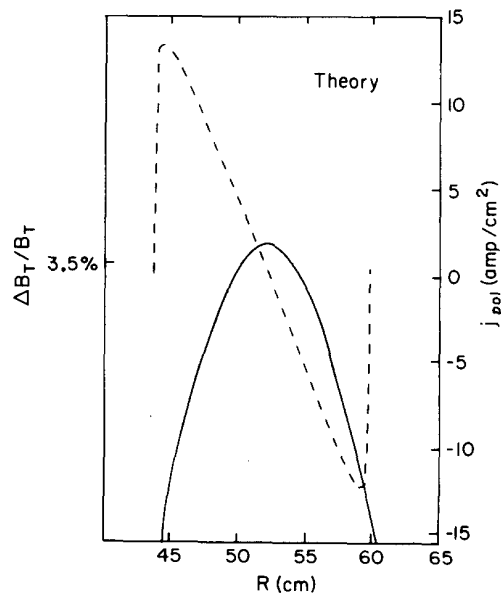


FIG. 3. Equilibrium code predictions for the fractional change in toroidal magnetic field $\Delta B_T/B_T$ (solid line) due to plasma and poloidal current density j_p (dashed line) as a function of distance from the major axis.

ment, $p'(\psi) = \partial p / \partial \psi$ is negligible and may be ignored. $F(\psi) = rB_z$ is prescribed in the plasma to be $F(\psi) = [1 + g(\psi - \psi_i / \psi_m - \psi_i)^\alpha]$, where ψ_i is the limiting flux surface, ψ_m is the value of the poloidal flux function ψ at the central magnetic axis, α is a shaping parameter set equal to 1.1, g is adjusted to keep the total current constant, and F_v is a constant equal to F in the vacuum region. An initial guess at $\psi(r, z)$ is used to evaluate $F(r, z)$. The operator Δ^* is then inverted subject to the boundary conditions that ψ be constant on the rings and walls. F is recalculated with the new $\psi(r, z)$ and the process is repeated until $\psi(r, z)$ converges. The limiting flux surface ψ_i is taken to be the divertor separatrix. The solution for $\psi(r, z)$ and the magnetic surfaces has previously been verified through direct experimental measurements.^{2,3}

The calculation predicts (Fig. 3) the change in toroi-

dal field ΔB_z to be roughly 3.5%. In order to accurately compare with theory which excludes current in the scrape-off region, it is necessary to discount the contribution of current outside the separatrix to ΔB_z . Thus for comparison, ΔB_z should be measured from the dashed baseline drawn in Fig. 2. The ΔB_z below the baseline (which intersects the curve at the separatrix) is due entirely to the current outside the separatrix. Experiment and code calculations agree well.

¹J. D. Callen and R. A. Dory, *Phys. Fluids* **15**, 1523 (1972).

²A. P. Biddle, R. N. Dexter, R. J. Groebner, D. J. Holly, B. Lipschultz, M. W. Phillips, S. C. Prager, and J. C. Sprott, *Nucl. Fusion* **19**, 1509 (1979).

³B. Lipschultz, S. C. Prager, T. H. Osborne, J. C. Sprott, and M. W. Phillips, *Phys. Rev. Lett.* **43**, 36 (1979).

Nonlinearly stable equilibrium statistical states for spheromaks

George Vahala

Department of Physics, College of William and Mary, Williamsburg, Virginia 23185
(Received 28 June 1979; accepted 30 October 1979)

Even though the eigenfunctions of the curl operator do not form a complete set, one still obtains the force-free spheromak field as the only nonlinearly stable state for spherical plasmas.

In recent papers¹⁻³ on incompressible magnetohydrodynamic turbulence and the nonlinear stability criterion which readily emerged from these statistical calculations, an assumption was made that the eigenfunctions of the curl operator, $\nabla \times \mathbf{F} = \lambda \mathbf{F}$ with $\mathbf{F} \cdot \hat{\mathbf{n}} = 0$ at the conducting wall, formed a complete set for solenoidal vector fields. It now appears that this assumption is incorrect. In this note, we rectify this error for spherical plasmas (spheromak⁴), using the notation of Ref. 3.

We expand the magnetic and velocity vector potentials \mathbf{A} and \mathbf{A}_v , terms of the vector fields⁵ \mathbf{M}_{nmq} and \mathbf{N}_{nmq} generated from the eigenfunctions of the scalar wave equation $\nabla^2 \psi + \lambda^2 \psi = 0$ by $\mathbf{M}_{nmq} = \nabla \times (\psi_{nmq} r \hat{\mathbf{r}})$ and $\mathbf{N}_{nmq} = \lambda_{nq}^{-1} \nabla \times \mathbf{M}_{nmq}$, i.e.,

$$\mathbf{A} = \sum (\xi_{nmq}^{(1)} [e] \mathbf{M}_{nmq} [e] + \xi_{nmq}^{(2)} [e] \mathbf{N}_{nmq} [e]) c_{nmq}, \quad (1)$$

$$\mathbf{B} = \nabla \times \mathbf{A} = \sum \lambda_{nq} c_{nmq} (\xi_{nmq}^{(1)} [e] \mathbf{N}_{nmq} [e] + \xi_{nmq}^{(2)} [e] \mathbf{M}_{nmq} [e]), \quad (2)$$

$$\mathbf{V} = \nabla \times \mathbf{A}_v = \sum \lambda_{nq} c_{nmq} (\eta_{nmq}^{(1)} [e] \mathbf{N}_{nmq} [e] + \eta_{nmq}^{(2)} [e] \mathbf{M}_{nmq} [e]), \quad (3)$$

where

$$\mathbf{M}_{nmq} [e] \equiv \frac{m}{\sin \theta} j_n P_n^m \begin{bmatrix} -\sin m \phi \\ \cos m \phi \end{bmatrix} \hat{\theta} - j_n \frac{\partial P_n^m}{\partial \theta} \begin{bmatrix} \cos m \phi \\ \sin m \phi \end{bmatrix} \hat{\phi}, \quad (4)$$

$$\mathbf{N}_{nmq} [e] \equiv \frac{n(n+1)}{\lambda_{nq} r} j_n P_n^m \begin{bmatrix} \cos m \phi \\ \sin m \phi \end{bmatrix} \hat{r} + \frac{1}{\lambda_{nq} r} \frac{d}{dr} (r j_n) \times \left\{ \frac{\partial P_n^m}{\partial \theta} \begin{bmatrix} \cos m \phi \\ \sin m \phi \end{bmatrix} \hat{\theta} + \frac{m}{\sin \theta} P_n^m \begin{bmatrix} -\sin m \phi \\ \cos m \phi \end{bmatrix} \hat{\phi} \right\}, \quad (5)$$

with

$$\nabla \times \mathbf{M}_{nmq} [e] = \lambda_{nq} \mathbf{N}_{nmq} [e], \quad (6)$$

$$\nabla \times \mathbf{N}_{nmq} [e] = \lambda_{nq} \mathbf{M}_{nmq} [e]. \quad (7)$$

The eigenvalues λ_{nq} are determined from the boundary conditions $B_r = 0 = v_r$ at the wall $r = a$, i.e., λ_{nq} is the q th zero of

$$j_n(\lambda_{nq} a) = 0. \quad (8)$$

The two sets

$$\{\mathbf{M}_{nmq} [e]\}, \{\mathbf{N}_{nmq} [e]\}$$

are orthogonal

$$\int \mathbf{M}_{nmq} [e] \cdot \mathbf{N}_{n'm'q'} [e] d^3x = 0,$$

while

$$\int \mathbf{M}_{nmq} [e] \cdot \mathbf{M}_{n'm'q'} [e] d^3x = 0 = \int \mathbf{N}_{nmq} [e] \cdot \mathbf{N}_{n'm'q'} [e] d^3x$$

trivially, for all n, n', m, m', q, q' . The c_{nmq} are the normalization constants with the property